Hindawi
Journal of Engineering
Volume 2022, Article ID 6006810, 7 pages
https://doi.org/10.1155/2022/6006810

Research Article

Design and Analysis of Combined Valve Spool with Linear Flow Coefficient

Changxiong Xie,[1] Heng Su,[2] Jun Yang ,[2] and Zhongjing He[2]

[1]*Key Laboratory of Air-Driven Equipment Technology of Zhejiang Province, College of Mechanical Engineering, Quzhou University, Kecheng District, Quzhou City 324000, China*
[2]*College of Engineering and Design, Hunan Normal University, College of Engineering and Design, Taozihu Road, Yuelu District, Changsha 410081, China*

Correspondence should be addressed to Jun Yang; yangcsu@126.com

Received 8 December 2021; Revised 10 April 2022; Accepted 7 May 2022; Published 13 June 2022

Academic Editor: Muhammed Hassan

The orifice flow model is generally established based on the turbulent state, and the flow discharge is considered to be a constant value. In fact, the flow discharge has obvious nonlinearity under the condition of small opening and small pressure difference of the valve port, which makes the electro-hydraulic servo system more difficult to control. In order to improve the nonlinearity of the flow discharge, the paper designed different spool profile, such as the arc combined spool profile, the power curve combined spool profile, the index curve combined spool profile, and the mixed curve combined spool profile, and analyzed the flow discharge through CFD simulation and experiment. The results show that the flow discharge of the mixed curve combined spool is more linear and the residual sum of squares is the smallest, which is 2.56×10^{-3} under CFD numerical simulation and 3.26×10^{-4} under experiment. The combined spool has better linear characteristics, which can improve the control performance of the electro-hydraulic servo valve.

1. Introduction

Due to the high-power mass ratio and large load driving capability, the hydraulic system is widely used in industrial, military, aerospace, and other fields [1, 2]. However, the inherent nonlinearity and uncertainty of the hydraulic system will deteriorate its control performance, resulting in the decrease of the overall performance of the equipment finally. Therefore, how to deal with the nonlinearity and uncertainty of the hydraulic system is an important research field of hydraulic control [3–6].

Usually, the control performance of the hydraulic system is improved by using nonlinear algorithms, such as fuzzy control, sliding mode control, neural network control, and so on. For example, Lee et al. [7] designed an adaptive fuzzy controller to adjust the opening of a servo valve and improve the accuracy of the workpiece. A sliding mode observer and a high-order sliding mode observer for hydraulic actuators were presented considering different sets of available measurements, parametric uncertainties, and model nonlinearities in [8]. Kim et al. [9] proposed a control method with an inverse model composed of a deep neural network, which accurately tracks a force trajectory. Zeng et al. [10] used the principle of structural invariance to design the compensation controller, which compensated the nonlinear flow of the proportional servo valve affected by pressure difference, opening size, interference, and other factors, so that the output flow characteristic of the proportional servo valve is linear.

However, few advanced control algorithms consider the nonlinearity of flow coefficient for its complexity. Actually, the nonlinearity of spool flow coefficient is one of the important factors in hydraulic nonlinearity. In

engineering practice, most researchers regard the flow coefficient in the flow formula of thin-walled small holes as a constant, while in practice, when the opening amount of the spool valve is small or the pressure difference is small, the flow coefficient is a nonlinear variable [11]. For example, the flow coefficient shown in equation (1) is not a constant, which changes with the valve structure and flow parameters [12].

$$\begin{cases} C_d = \left(2.28 + 64\dfrac{2L}{d_0 d}\right)^{-1/2} \left(\dfrac{d_0 d}{2} \le 50\right), \\ C_d = \left[1.5 + 13.74\left(\dfrac{2L}{d_0 d}\right)^{1/2}\right]^{-1/2} \left(\dfrac{d_0 d}{2} > 50\right), \end{cases} \tag{1}$$

where L is the hole length, d is the tube diameter, and d_0 is the hole diameter. Ji et al. [13] designed the flow area at the valve port of the two-section rectangular throttling groove as the coupling function of the valve port area and the flow coefficient based on the series-parallel effect of the throttling surface in the throttling groove. The flow coefficient at the valve port has a piecewise linear characteristic, which reasonably shows the control effect of the valve port geometric area and the valve port shape on the flow [14]. Zeng et al. [15] proposed a compensator by solving the equation of the novel flow and desired flow considering the change of flow coefficient.

Actually, the hydraulic valve with linear flow coefficient can reduce the complexity of the control strategy and improve the control accuracy. However, there is no related research about how to design the spool with linear characteristics [16]. In this paper, different combined profiles of the spools were designed to improve the linear characteristic of the flow.

The rest of this article is organized as follows. Section 2 describes the structure of the combined valve spool. Sections 3, 4, and 5 comprise the detailed numerical model and grid independence verification and some simulation results. The experiment results are reported in Section 6. Finally, conclusions are furnished in Section 7.

2. Structure and Equations of Combined Valve Spool

The main structure of the seat valve that includes the spool and seat is shown in Figure 1. The contact area between the spool and seat is a curved surface. The curved surface is formed by the rotation of the generatrix. The flow rate through the poppet valve is determined by the external parameters and the shape of the contact curved surface area.

According to the geometric structure and flow characteristics of the seat valve, the governing equation can be established as

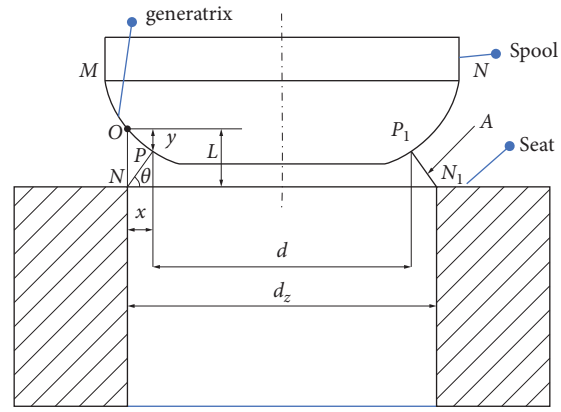

Figure 1: Seat valve structure.

$$\begin{cases} d = d_z - 2x, \\ A = \pi\left(\dfrac{d_z}{2} + \dfrac{d}{2}\right)\dfrac{x}{\cos\theta}, \\ Q = Av, \\ \dfrac{\Delta P}{\rho g} = \dfrac{v_2^2 - v_1^2}{2g}, \\ C_d = \dfrac{Q}{A}\sqrt{\dfrac{\rho}{2\Delta P}}, \\ L = y + x\tan\theta, \end{cases} \tag{2}$$

where Q, A, v, v_2, v_1, g, and ρ are flow, discharge area, velocity in cross section, inlet velocity, outlet velocity, acceleration of gravity, and fluid density, respectively. L is the opening size, x is the abscissa, and y is the ordinate. C_d is the flow coefficient. d_z is the diameter of the valve seat. Other symbols are shown in Figure 1. According to equation (2), the generatrix equation of the spool is

$$x^2 + \frac{x d_z}{4\pi C_d}\sqrt{\frac{\pi^2 C_d^2 d_z^2 - 4\pi}{x^2 + y^2}} - d_z x = 0. \tag{3}$$

Set $F = x^2 + (xd_z/4\pi C_d)\sqrt{(\pi^2 C_d^2 d_z^2 - 4\pi/x^2 + y^2)} - d_z x$. In order to meet gliding property of the spool generatrix, F needs to satisfy the following equation:

$$\begin{cases} F = x^2 + \dfrac{d_z\cos\theta}{4\pi C_d}\sqrt{\pi^2 C_d^2 d_z^2 - 4\pi} - d_z x = 0, \\ \dfrac{\partial F}{\partial\theta} = 0. \end{cases} \tag{4}$$

In order to obtain the valve spool structure with linear flow coefficient, the form of flow coefficient can be set as

$C_d = aL + b$, where a and b are both constants. Then, equation (5) is derived from equation (4).

$$\begin{cases} \underbrace{x^2 + d_z \cos\theta \cdot \sqrt{\pi^2 (aL+b)^2 d_z^2 - 4\pi}/4\pi(aL+b)}_{s1} \underbrace{-d_z x}_{s2} = 0, \\ L = y + x\tan\theta, \\ \dfrac{\partial F}{\partial \theta} = 0. \end{cases} \tag{5}$$

Equation (5) is solved, and the result is shown as follows.

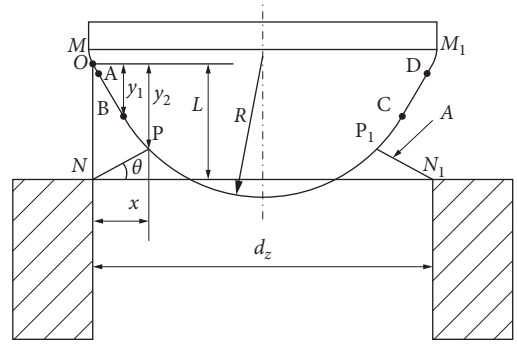

Figure 2: Arc combined spool structure.

$$\begin{cases} F = x^2 + \dfrac{d_z \cos\theta}{4\pi(ay + ax\tan\theta + b)} \sqrt{\pi^2 (ay + ax\tan\theta + b)^2 d_z^2 - 4\pi} - d_z x = 0, \\ \dfrac{\partial F}{\partial \theta} = \dfrac{\partial \left[x^2 + \left(d_z \cos\theta / 4\pi (ay + ax\tan\theta + b) \right) \sqrt{\pi^2 (ay + ax\tan\theta + b)^2 d_z^2 - 4\pi} - d_z x \right]}{\partial \theta} = 0. \end{cases} \tag{6}$$

When the opening size L is determined, firstly, the value of θ can be solved by using equation (6). Then, equation (6) can be solved. Lastly, the equation of the combined spool generatrix can also be obtained.

From equation (5), when the opening degree L and θ are determined, the part s_1 of equation (5) can be described as follows:

$$x^2 + x\tan\theta + c \cdot d - L = 0, \tag{7}$$

where $c = (d_z \cos\theta / 4\pi(aL+b))$ and $d = \sqrt{\pi^2 (aL+b)^2 d_z^2 - 4\pi}$. Part s_2 can be described as

$$-d_z x - x\tan\theta + L = 0, \tag{8}$$

and equation (7) represents a curve and equation (8) represents a line approximately from these equation forms.

According to equations (7) and (8), this paper proposed the curve and line combined generatrix to approximate the ideal curve which is described in equation (6). To simplify the analysis, an arc was chosen to represent a special curve. And a new spool structure combining arc and line are shown in Figure 2.

The rear sections AB and CD are lines, the front section BC is an arc, and the MA and M'D sections are the transitional arcs used for connection. The transitional arcs have little effect on the structure of the combined spool. The equations of the generatrix of the AB and BC segments are

$$\begin{cases} y_1 = \sqrt{3}\, x_1 + m, \\ y_2 = \sqrt{R^2 - \left(\dfrac{d_z}{2} - x_2 \right)^2} - n. \end{cases} \tag{9}$$

Both m and n are constants, and R is the radius of the arc. Based on the arc combined spool in Figure 2, this paper constructed two new-type spools. The shape of the generatrix of the new structure spool was close to that of the arc combined spool. The curves of these two spools are the power polynomial curve (abbreviated as power curve) and index function curve (abbreviated as index curve). The equations of the two curves are shown in equations (10) and (11), respectively. The structures of these two spool heads are shown in Figure 3 as b and c.

$$y = 0.0015x^3 + 0.021x^2 - 0.01x, \tag{10}$$

$$y = 0.012e^x. \tag{11}$$

Based on equations (10) and (11), the equations of the power curve and the index curve were mixed and added, and the coefficients were rectified to obtain a mixed function curve (abbreviated as mixed curve). The equation of the curve is shown in equation (12). The spool head structure is shown in Figure 3 as a.

$$y = 0.0012e^x + 0.0015x^3 + 0.15x^2 - 0.01x. \tag{12}$$

3. Numerical Calculation

3.1. Numerical Simulation Settings. Settings of flow field boundary conditions are as follows. (1) The $k - \varepsilon$ turbulence model was selected as the calculation model. (2) No. 46 wear-resistant hydraulic oil was selected as the medium, with density of 870 kg/m^3 and dynamic viscosity of 0.03915 kg/ms. (3) The inlet pressure is set up as 4 MPa and the outlet pressure is 0.5 MPa.

The flow coefficient formula is

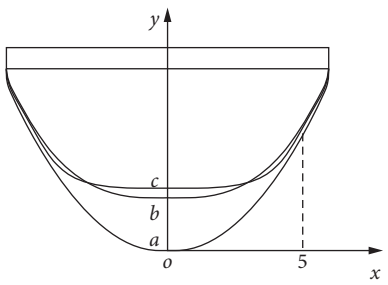

Figure 3: Schematic diagram of curve: (a) mixed curve, (b) power curve, and (c) index curve.

$$C_d = \frac{Q}{A}\sqrt{\frac{\rho}{2\Delta p}}, \tag{13}$$

where Q is the volumetric flow, A is the flow area, ρ is the fluid density, and Δp is the pressure difference.

The fluid domain flow is set as 3D model, steady and incompressible flow, and the fluid flow needs to meet the governing equations which included the continuity equation (14) and momentum equation (15).

$$\frac{\partial u}{\partial x} + \frac{\partial v}{\partial y} + \frac{\partial w}{\partial z} = 0, \tag{14}$$

$$\begin{cases} \rho\left(u\dfrac{\partial u}{\partial x} + v\dfrac{\partial u}{\partial y} + w\dfrac{\partial u}{\partial z}\right) = \mu\left(\dfrac{\partial^2 u}{\partial x^2} + \dfrac{\partial^2 u}{\partial y^2} + \dfrac{\partial^2 u}{\partial z^2}\right) - \dfrac{\partial p}{\partial x}, \\ \rho\left(u\dfrac{\partial v}{\partial x} + v\dfrac{\partial v}{\partial y} + w\dfrac{\partial v}{\partial z}\right) = \mu\left(\dfrac{\partial^2 v}{\partial x^2} + \dfrac{\partial^2 v}{\partial y^2} + \dfrac{\partial^2 v}{\partial z^2}\right) - \dfrac{\partial p}{\partial y}, \\ \rho\left(u\dfrac{\partial w}{\partial x} + v\dfrac{\partial w}{\partial y} + w\dfrac{\partial w}{\partial z}\right) = \mu\left(\dfrac{\partial^2 w}{\partial x^2} + \dfrac{\partial^2 w}{\partial y^2} + \dfrac{\partial^2 w}{\partial z^2}\right) - \dfrac{\partial p}{\partial z} - \rho g, \end{cases} \tag{15}$$

where u, v, and w are the velocity components on the three coordinate axes of x, y, and z.

The inlet and outlet diameters of the fluid domain are both 6 mm, and the CFD tetrahedral mesh was automatically generated by mesh, and the size was set to 2 mm. Due to the study of the flow coefficient at the valve port, the mesh at the valve port needs to be refined, so the mesh size was set to 0.5 mm, and the refined fluid domain mesh is shown in Figure 4.

3.2. Grid Independence Verification. The grid independence verification can reduce the influence of the number and quality of the grid on the results. This paper calculated the half-channel outlet flow with the number of grids between 300,000 and 1.2 million, as shown in Table 1. After the number of refined grid cells reached 600,000, the outlet flow fluctuated around 36.91 L/min, and the flow rate changed little, while the grid quality was also maintained at around 0.88. In order to reduce the amount of calculation, the number of finite element meshes is limited to 600, 00.

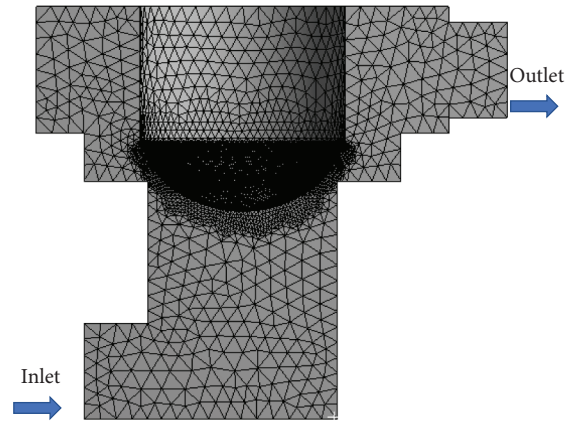

Figure 4: Fluid domain model.

Table 1: Grid independence verification.

Number	Number of grid cells	Grid unit quality	Outlet flow Q (L/min)
1	307989	0.75	36.20
2	632758	0.88	36.91
3	950184	0.88	36.93
4	1206332	0.88	36.95

4. Calculation of Flow Area

The position of the flow area of the valve port is the narrowest area. Also, the liquid velocity reaches the maximum. The velocity streamline diagram of the combined valve port was obtained by calculation as shown in Figure 5(a). The detection showed that the direction of the maximum velocity at the valve port was parallel to the cone of the circular arc combined spool, and the hydraulic oil velocity streamline at the combined valve port is shown in in Figure 5(a), and the position of the flow area is A_1B_1. Figure 5(b) shows a schematic diagram of the flow area of the combined valve port. Since the line in the generatrix of the combined valve spool constitutes the cone of the combined valve spool, the principle of determining the flow section is the same.

Then, the flow area can be determined according to the geometric structure of the valve [6].

$$\begin{cases} S = S = \pi d_z x \sin\alpha\left(1 - \dfrac{x}{d_z}\sin\alpha\cos\alpha\right), & (x < x_l), \\ S = \pi\left(x\sin\alpha\cos\alpha + d_f - 2H\tan\alpha\right)x\sin\alpha, & (x > x_l), \end{cases} \tag{16}$$

where x_l is the opening degree.

$$x_l = \frac{d_z - d_f + 2H\tan\alpha}{\sin(2\alpha)}, \tag{17}$$

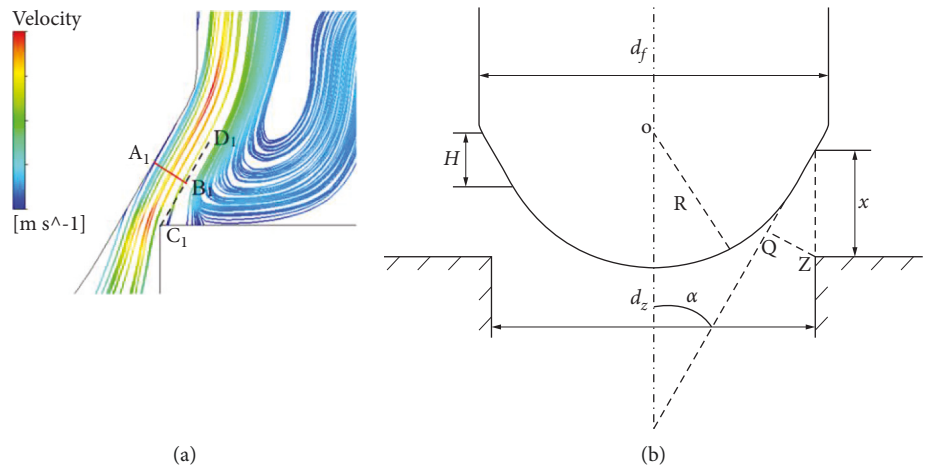

Figure 5: Combined valve port flow area. (a) Streamline diagram of combined valve port speed. (b) Schematic diagram of the flow area of the combined valve.

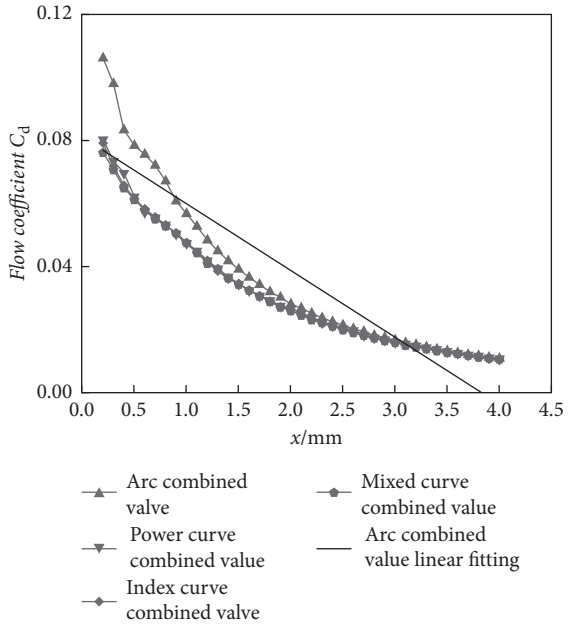

Figure 6: Flow coefficient of four valves.

where α is the half cone angle of the spool, H is the cone height, x is the opening degree, d_f is the spool diameter, and d_z is the diameter of the valve seat.

5. Simulation of Flow Coefficient

The flow coefficient curves of the four combined valves are shown in Figure 6. The flow coefficients of the four spools gradually decrease with the increase of the opening degree similarly.

The maximum flow coefficient is near 0.12 at the moment the spool opens. When opening degree approaches to 4 mm, the coefficient nears 0.02. Then, the coefficient tends to stabilize.

Table 2: Sum of residual squares for flow coefficient ($\times 10^{-3}$).

Spool structure	Residual sum of squares
Arc	3.77
Power curve	1.57
Index curve	1.44
Mixed curve	1.29

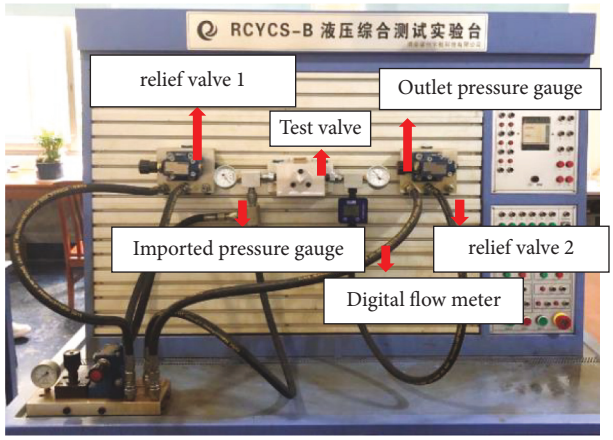

Figure 7: Experimental platform.

To analyze the linearity of the flow coefficient deeply, the flow coefficients of the spools of different contours were linearly fitted. Four different discharge coefficient curves and a fitting curve of an arc are described in Figure 6.

Residual sum of squares (RSS) essentially determines how well a regression model explains or represents the data in the model.

$$RSS = \sum_{1}^{n} \left(y^i - f\left(x_i\right)\right)^2, \tag{18}$$

(a) (b)

Figure 8: The actual test spool. (a) The actual value spool. (b) Enlarged view of spool head.

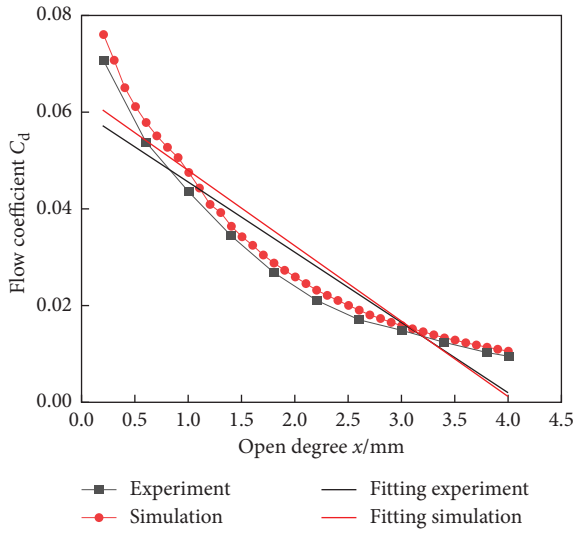

Figure 9: Flow coefficient of mixed curve.

where y^i is the i^{th} value of the variable to be predicted, $f(x^i)$ is the predicted value of y^i, and n is the upper limit of summation.

Within the range of the spool stroke, the linear characteristic of the flow coefficient is all segmented, and the residual sum of squares was obtained by fitting as shown in Table 2.

The power curve index curve and mixed curve combined valve flow coefficient curve are close, and the residual sum of the flow coefficient residuals of the mixed curve combined valve is 1.29×10^{-3}, which proves that the combined valve port flow coefficient of the mixed curve in the combined valve has a good linear characteristic, which verifies the effectiveness of the combined valve spool design method.

6. Experimental Verification

The platform includes hydraulic system, pressure and flow measurement system, and valve to be tested system. The experimental platform is shown in Figure 7. Relief valve is used to adjust the inlet and outlet pressure, a pressure gauge is used to measure the pressure of the inlet and outlet, the digital flow meter is used to measure the outlet flow, and the test valve contains test spools.

Table 3: Sum of squares of residuals for experiment and simulation ($\times 10^{-3}$).

Spool structure	Simulation	Experiment
Arc	3.77	1.29
Power curve	1.57	0.389
Index curve	1.44	0.368
Mixed curve	1.29	0.326

The processed spools are shown in Figure 8(a), and the enlarged shape of the spool head is shown in Figure 8(b).

The flow coefficient characteristics of the four processed spools were verified by experiment and simulation. Figure 9 compares the flow coefficient curve and fitting curve of experiment and simulation, respectively, of mixed curve. It can be seen from the figure that there is a big error when the opening is small. When the opening is large, the two fitted straight lines are basically consistent.

In order to better show the approximation degree of different curves, the sum of squares of residuals between the fitting curve and the actual curve is analyzed. Also, the results of the sum of squares of flow coefficient residuals under physical experiment and numerical simulation are shown in Table 3.

According to the two research methods of numerical simulation and experiment, there is a certain error in the residual squares of the flow coefficient because of the hydraulic sealing and machining accuracy of the test valves. Under the experimental method, the sum of squares of the flow coefficient of the mixed curve combined valve is also a minimum of 3.26×10^{-4}, which shows the effectiveness of the combined spool design method.

Although the simulation results are inconsistent with the experimental results, the trend is consistent. In fact, the difference of flow coefficient between the two is very small.

7. Conclusion

(1) A design method of spool structure based on linear flow coefficient is proposed. Through modeling and

numerical analysis, the combined spool structure with linear flow coefficient is deduced and obtained. The front section of the generatrix is a curve, and the rear section is a line.

(2) Four different combined spool structures are proposed and compared. In these spools, the minimum residual sum of squares of the flow coefficient of the mixed curve combined valve is 2.56×10^{-3}. Mixed curve combined valve under experiment is also small (3.26×10^{-4}), which is the best spool structure with linear coefficient.

Data Availability

No data were used to support this study.

Conflicts of Interest

The authors declare that they have no conflicts of interest.

Acknowledgments

This research was funded by the Outstanding Youth Project of Hunan Provincial Department of Education (19B348).

References

[1] J. Koivum and J. Mattila, "High performance nonlinear motion/force controller design for redundant hydraulic construction crane automation," *Automation in Construction*, vol. 51, no. 1, pp. 59–77, 2015.

[2] L. Sidho, X. Brum, M. Smaoui, E. Bideaux, and E. Thomasset, "Dynamic gains differentiator for hydraulic system control," *Journal of Dynamic Systems, Measurement, and Control*, vol. 137, no. 4, pp. 04101–04107, 2015.

[3] H. Yan and Y. Zhu, "Bang-bang control model for uncertain switched systems," *Applied Mathematical Modelling*, vol. 15, no. 1, pp. 1–10, 2014.

[4] S. Wang, "Generic modeling and control of an open circuit piston pump part I: theoretical model and analysis," *Journal of Dynamic Systems, Measurement, and Control*, vol. 138, no. 4, pp. 041001–041004, 2016.

[5] E. Jalayeri, A. Imam, and N. Sepehri, "A throttle-less single rod hydraulic cylinder positioning system for switching loads," *Case Studies in Mechanical Systems and Signal Processing*, vol. 1, no. 2, pp. 27–31, 2015.

[6] J. Mattila, J. Koivumäki, D. G. Caldwell, and C. Semini, "A survey on control of hydraulic robotic manipulators with projection to future trends," *IEEE*, vol. 22, no. 2, pp. 669–680, 2017.

[7] Y. H. Lee, J. C. Thurmon, G. J. Benson, W. T. Tranquilli, and S. Crotchik, "The systemic and regional hemodynamic effects of dopamine, dobutamine, dopexamine and 5% dextrose in sevoflurane anesthetized dogs," *Veterinary Anaesthesia and Analgesia*, vol. 28, no. 2, p. 99, 2001.

[8] G. Palli, S. Strano, and M. Terzo, "Sliding-mode observers for state and disturbance estimation in electro-hydraulic systems," *Control Engineering Practice*, vol. 74, no. 3, pp. 58–70, 2018.

[9] S. W. Kim, B. Cho, S. Shin, J. H. Oh, J. Hwangbo, and H. W. Park, "Force control of a hydraulic actuator with a neural network inverse model," *IEEE Robotics and Automation Letters*, vol. 6, no. 2, pp. 2814–2821, 2021.

[10] L. Zeng, J. Yang, and J. Tan, "Compensation control of a nonzero open valve controlled asymmetric cylinder system based on model invariance," *Huazhong University of Science and Technology*, vol. 45, no. 3, pp. 32–34, 2017, in Chinese.

[11] K. Ramamurthi and K. Nandakumar, "Characteristics of flow through small sharp-edged cylindrical orifices," *Flow Measurement and Instrumentation*, vol. 10, no. 3, pp. 133–143, 1999.

[12] L. Zeng, J. Yang, and J. Tan, "Compensator designed for electro-hydraulic servo system in laminar state," *Mechanics*, vol. 27, no. 2, pp. 107–114, 2021.

[13] H. Ji, J. H. Zhang, and D. Wang, "Flow control characteristic of the orifice *S*-pool valve with notches," *Transactions of the Chinese Society for Agricultural Machinery*, vol. 40, no. 1, pp. 199–202, 2009, in Chinese.

[14] V. Milic, Ž. Šitum, and M. Essert, "Robust position control synthesis of an electro-hydraulic servo system," *ISA Transactions*, vol. 49, no. 4, pp. 535–542, 2010.

[15] L. Zeng, J. P. Tan, and J. Yang, "Load flow property of electrohydraulic proportional valve controlling asymmetric cylinder system," *Journal of Central South University*, vol. 47, no. 7, pp. 2282–2285, 2016, in Chinese.

[16] S. Li, J. Ruan, and B. Meng, "Dither compensation for dead zone of zero load flow of characteristics," *Journal of Mechanical Engineering*, vol. 50, no. 18, p. 186, 2014, in Chinese.